Functionally graded Ti6Al4V-Mo alloy manufactured with DED-CLAD ® process

Catherine Schneider-Maunoury, Laurent Weiss, Philippe Acquier, Didier Boisselier, Pascal Laheurte

Functionally graded Ti6Al4V-Mo alloy manufactured with DED-CLAD® process

Catherine Schneider-Maunoury[a,b,*], Laurent Weiss[b], Philippe Acquier[a], Didier Boisselier[a], Pascal Laheurte[b]

[a] Irepa Laser, Parc d'Innovation Pôle API, 320 Boulevard Sébastien Brant, 67400 Illkirch, France
[b] LEM3, Université de Lorraine, 7 Rue Félix Savart, 57013 Metz, France

ARTICLE INFO

Keywords:
Additive manufacturing
Functionally graded material
Direct energy deposition
Microstructure
Ti6Al4V-Mo alloys

ABSTRACT

This paper presents the results of functionally graded Ti6Al4V-Mo alloy manufactured with directed energy deposition called CLAD® (Construction Laser Additive Direct) process. Single track width sample with five gradients of composition, from 0 to 100 wt.% Mo, was manufactured using a coaxial nozzle. Both Ti6Al4V and Mo ratios were modified with a 25 wt.% increase or decrease in the chemical composition of each gradient. A two-powder feeder was used to input the correct ratio of each powder, so as to obtain the desired chemical composition. XRD analysis allowed to define the phases present in each deposition, as well as the lattice parameter. SEM observations showed microstructural evolution from 25 wt% Mo on, namely where the β-phase becomes dominant. Moreover, dendrites appear from 50 wt.% Mo on. Microhardness analysis revealed variation along the deposition depending on the chemical composition. The homogeneity of the powder mixture under laser beam was highlighted thanks to tomography on the manufactured samples, which validates the processability of functionally graded material (FGM) by CLAD® process.

1. Introduction

Additive manufacturing (AM) was developed during the eighties and is currently used by companies in numerous sectors such as the biomedical sector, aerospace, as well as automotive prototyping. In AM process, a part is created by adding layers of materials, contrary to conventional process such as machining which consists in removing material from a blank. There are two types of AM metallic processes: Powder Bed Fusion processes such as Selective Laser Melting/Sintering (SLM/SLS), and Directed Energy Deposition (DED) processes such as Laser Engineered Net Shaping (LENS) or Construction Laser Additive Direct (CLAD). In all of these processes, parts are manufactured layer-by-layer to obtain the required geometry. Initially developed for prototyping, AM is now used in parts production. However, these technological processes are less productive than usual machining, and thus are more adapted to part production in small series [1]. DED process has a wide and promising range of applications such as the manufacturing of large parts and the repair of existing parts [2].

Functionally Graded Materials (FGM) were developed to associate and concentrate the benefits of physical and mechanical properties of two or more materials into one part. During the manufacturing of such materials, the chemical composition of the deposited material is modified gradually by adjusting the ratio of different alloys injected and melted under the laser beam. Therefore, mechanical and microstructural properties gradually vary along one or more space directions. These types of materials are suitable candidates for numerous high tech applications such as nuclear industry, aerospace and bioengineering [3]. In the CLAD® process, as the powders are injected in the laser beam, and contrary to powder bed fusion techniques, the manufacturing of functionally graded materials parts is made easier by using several powder tanks [4,5].

In the case of biomedical applications, Ti6Al4V is widely used because of its outstanding combination of strength, corrosion resistance, biocompatibility and low density [6]. Nevertheless, the difference in the Young Modulus of this alloy (106-108 GPa) is too large compared to that of the bone (10-30 GPa), creating a stress shielding effect which can lead to osteoporosis. Moreover, the Al and V elements contained in this alloy could cause long-term health

* Corresponding author at : Irepa Laser, Parc d'Innovation Pôle API, 320 Boulevard Sébastien Brant, 67400 Illkirch.
E-mail address: csm@irepa-laser.com (C. Schneider-Maunoury).

Table 1
Chemical composition of both Ti6Al4V and Mo powders.

	Molybdenum					Ti6Al4V			
Elements	Mo	Ti	V	W	O	Ti	Al	V	O
wt.%	>99.95	<0.05	<0.05	<0.05	0.013	<90	6	4	<0.13

damages in case of release into the body [7]. Furthermore, Ti6Al4V is combined with a non-toxic and non-allergenic Mo element which is a β-stabilizer and has lower Young's Modulus than α-phase.

FGM manufacturing is very complex with powder bed fusion process, while the CLAD® process allows to control the variation of the chemical composition at each step by the use of numerous powder feeders. Some alloys were already studied, namely:

- Inconel 718 on Ti6Al4V substrate [8] or functionally graded Ti6Al4V-Inconel 718 [9] where cracks appear due to the presence of intermetallic phases Ti_2Ni, TiNi, $TiNi_3$, TiFe and $TiFe_2$
- 304 L stainless steel - Invar 36 [4] and 316 L stainless steel - Invar [10] was well manufactured without defect
- 304L stainless steel - Inconel 625 [5] where cracks were found for approximately 79 wt.%SS304L and 21 wt.%IN625

Some authors have already worked on Ti6Al4V-Mo or Ti-Mo alloys by using AM process for biomedical applications such as orthopaedic implants or trauma surgery. However, they have limited their study to a maximum of 25 wt.% Mo amount in the deposition [11,12]. This paper is focused on Ti6Al4V-Mo alloy with a chemical composition which varied from 0 to 100 wt.% Mo with an increment of 25 wt.% Mo.

2. Materials

The baseplate is made of Ti6Al4V with dimensions of 100 mm × 100 mm × 8.8 mm. Ti6Al4V and Mo powders used in this study have a particle size ranging from 45 to 90 μm. The chemical composition of each powder is reported in Table 1. Ti6Al4 V powders were provided by TLS Technik and Mo powder by Tekna. As the difference in melting temperature between molybdenum and Ti6Al4V is high ($\Delta T \approx 950\,^{\circ}C$), the Mo powder was sieved in order to keep particles with a size distribution from 45 to 75 μm only. Fig. 1 shows the particle size distribution of both Ti6Al4V and Mo powder, but also the morphology.

3. Experimental procedure

FGMs samples were manufactured by differential injection using two powder feeders, each one containing a different material (Ti6Al4V and Mo). The powder ratio can be set for each material to meet the required chemical composition by adjusting the rotating speed of the powder feeder. Both materials are mixed before being injected in the laser beam. Then the melted particles are deposited onto the baseplate (Fig. 2). The chemical composition of the deposited material can be adjusted layer by layer to create a gradient of composition. The miscibility on Ti in Mo is total in β-phase at high temperature, as shown in phase-diagram [13]. A 2000 W laser diode was used, characterized by a 600 μm fibre diameter and a 980 nm wavelength. The energy distribution of the laser beam is homogenous and the laser beam profile is top hat in the focal plane. The diameter of the beam at the focus point is 2.2 mm. Manufacturing processes were carried out under argon gas due to the high affinity of Ti alloys with oxygen. Thanks to a gas purification system, O_2 level was maintained below 20 ppm and H_2O level below 50 ppm during manufacturing. The coaxial nozzle (developed by Irepa Laser, US patent n°5418350) was also adapted to be thicker and thus more resistant to very high temperature (>2000 °C). The cooling system of the nozzle was modified to improve its efficiency and thus to avoid problems such as nozzle clogging and meltdown.

The process parameters such as laser power, powder feed rate, travel speed and layer height step on z axis were adjusted according to the chemical composition. Thanks to the industrial experience of several years with the CLAD® technology, the main process parameters are well known and controlled for some materials such as Ti6Al4V and Mo. To manufacture a gradient of composition by mixing Ti6Al4V and Mo, a compromise was reached between the two laser power references for these two materials (internal data from Irepa Laser). Indeed, three laser powers were used to manufacture the wall: 1600, 1800 and 2000 W, for 100% Ti6Al4V, for the 3 different gradients of composition and for 100% Mo, respectively.

Samples were cut to analyse the cross-section along the manufacturing direction, and prepared for metallurgic observation by standard polishing methods and etching with Kroll solution for 10 s (95 ml demineralized water, 6 ml of HNO_3 and 3 ml of HF). The microstructures were observed by optical microscope and by scanning electron microscopy (FEG Zeiss Supra 40). The crystallographic orientation analysis was carried out by Electron Backscatter Diffraction (EBSD) with a W Jeol 6490 microscope and data were processed with AZtech (Oxford Instruments, HKL Technology). Meringue 2 software was used for the reconstruction of the β-phase, based on Burgers relationship [14]:

$$\{100\}_\beta // \{0002\}_\alpha, \langle 111\rangle_\beta // < 11\bar{2}0 >_\alpha$$

Chemical analysis was done by energy dispersive X-ray spectrometry (SEM-EDX) and data were processed with Esprit. The phases constitution of the alloys was determined by X-ray diffraction, using Bragg-Brentano diffractometer and Co Kα radiation ($\lambda_{k\alpha}$ = 1,78026 Å). Microhardness tests were made on a Buehler machine with 500 g load and 15 s of indentation time. Tomography tests were performed with Easytom Nano machine and data were processed with both WAct and Avizo software.

4. Results and discussion

4.1. Sample manufacturing

A single-track width wall was manufactured with 5 gradients of chemical composition using the CLAD® process (Fig. 3). In order to get at least two tracks with nominal composition which would not be influenced by dilution, 4 tracks were deposited for each gradient of composition. Deposition started with 100% Ti6Al4V at the bottom of the wall and finished with 100% Mo at the top. Both Ti6Al4V and Mo ratios were modified with a 25 wt.% increase or decrease in the chemical composition between each gradient. The final wall dimensions are 80 mm in length, 3 mm in width and 12 mm in height. Optical observations do not show any cracks or porosities.

4.2. Chemical analysis

Chemical analysis was performed by SEM-EDX to verify the amount of all elements in each gradient of composition (ie Ti, Al, V and Mo) depending on the programmed chemical composition. These analyses also allow to control the distribution of each chemical element present in the gradient of composition, and thus to ensure that the chemical composition is in accordance with the programmed ratio. Fig. 4 shows the variation in Ti, Al, V and Mo amounts at the interfaces between each gradient of composition. Results show that deposited layers with 100 wt.% Mo (Fig. 4a) presented a constant and correct chemical composition. The same observation can be made for the analyses across the baseplate in Ti6Al4V and the deposited layers with 100 wt.% Ti6Al4V (Fig. 4e). However, gradients from 25 wt.% to 75 wt.% Mo (Fig. 4b-d) reveal a

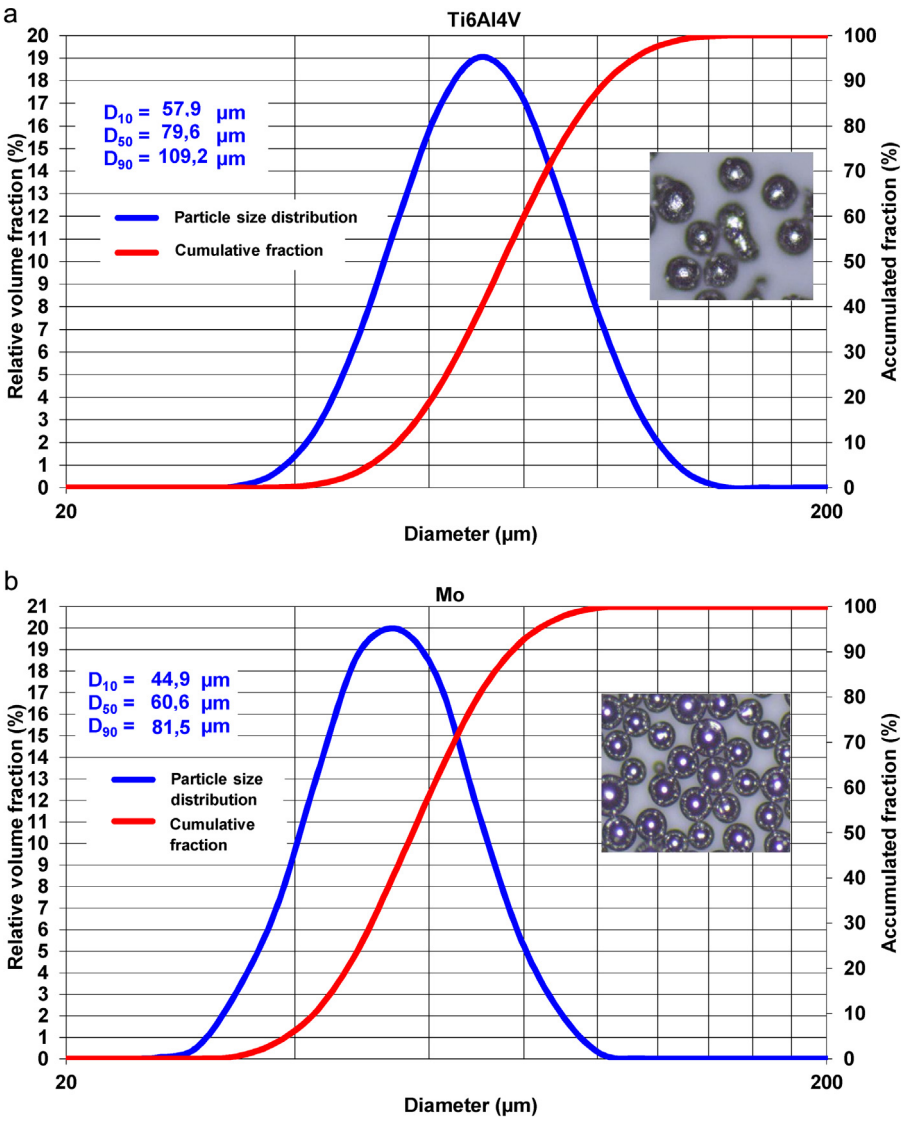

Fig. 1. Particle size distribution for (a) Ti6Al4V powder and (b) Mo powder.

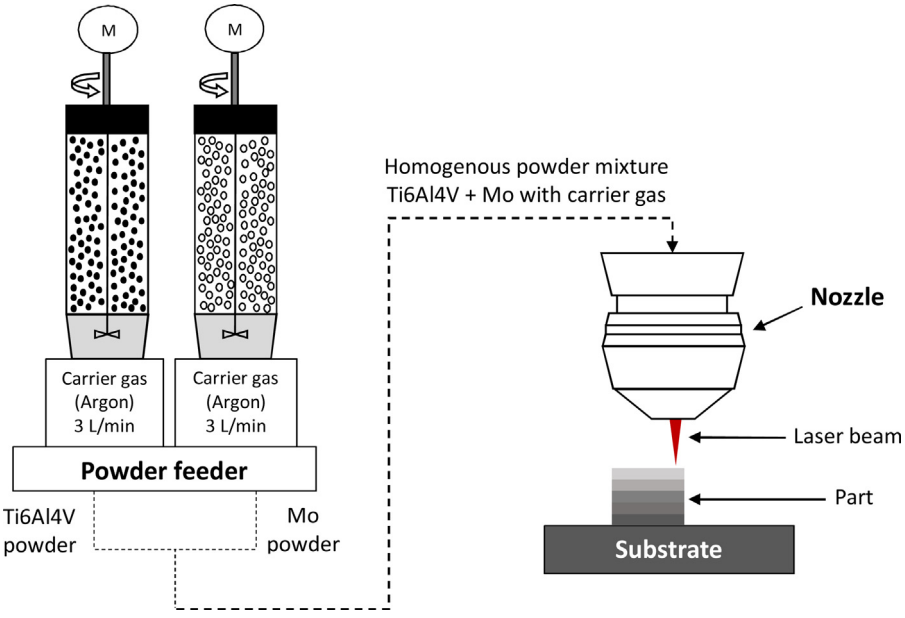

Fig. 2. Device assembly.

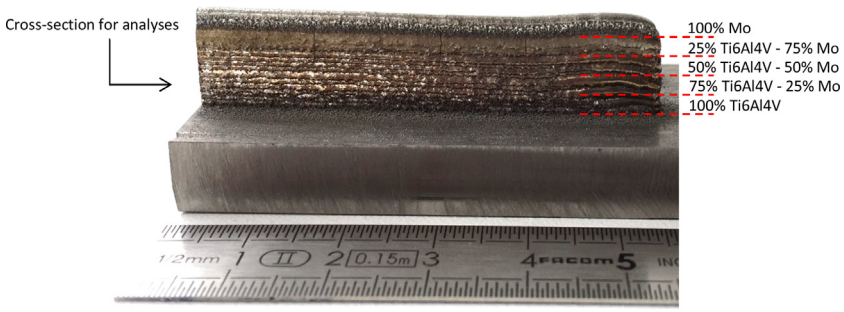

Fig. 3. Wall of functionally graded Ti6Al4V-Mo alloy with 25wt.% Mo increment.

difference of ~10% between the expected and the measured chemical composition. The presence of unmelted Mo particles in the deposition may be responsible for this gap between programmed and real compositions. Thus, the Mo content is lower than expected due to the presence of these unmelted Mo particles. Fig. 4 also revealed that transitions between each gradient are relatively soft.

Variation in the gradient composition from 50 wt.% and 75 wt.% Mo content can also be observed. This variation, more or less significant depending on the Mo amount, is explained by the dendritic substructure presented in the β-grains (Fig. 5). Indeed, light regions correspond to dendritic arms rich in Mo while the dark regions are rich in Ti. Fallah shows similar results with his work on TiNb alloy deposited with similar powder blown process [15], where white coarse dendrites are Nb-rich while the dark fine dendrites are Ti-rich regions. This is owing to a too low interaction time τ between the laser beam and the substrate as defined in Eq.(1):

$$\tau = D/V \tag{1}$$

where D is the laser beam diameter and V the travel speed. This beam interaction time may be insufficient to create a uniform liquid composition and two molten and chemically different regions cohabit when solidification starts. The metastable state of the β-phase may be another hypothesis for this difference in chemical composition.

Fig. 6 shows the repartition of Ti, Al, V and Mo along the deposition. Each transition between two gradients of composition is clearly visible, and the modification of the composition is observed by a higher or lower amount of elements. Then, the distribution of all elements in the deposition is homogeneous. Spherical unmelted particles are defined as molybdenum, which is confirmed by both EBSD and XRD analyses. These first results allow to validate the fact that the materials are well homogenised under the laser beam.

4.3. Microstructure

The crystallographic phases were indexed in the diffractogram in Fig. 7. Ti6Al4V baseplate presents α-phase (hexagonal structure) as well as a small fraction of β-phase (centred cubic structure), around 8%. This peak is hidden in the foot of α-phase peak. The 100 wt.% Ti6Al4V layers deposited present α'-phase with fine martensitic needle. The alloys containing up to 25 wt.% Mo consist of β-phase and Mo (centred cubic structure). Mo phase provides unmelted Mo particles. From 25 wt.% Mo content, β-phase of Ti6Al4V is dominant. The α'-phase initially present in the 100 wt.% Ti6Al4V disappears from 25 wt.% Mo. These results prove that molybdenum operates as a beta-gene element which avoids the martensitic transformation during cooling. These results also show that the β-phase is stabilized from 25 wt.% Mo content by using CLAD® process. Previous results show that a minimum of 10 wt.% Mo is required to stabilized β-phase [11,16]. As the chemical composition increased or decreased by a 25 wt% step in this study, it is difficult to identify this stabilization for 10 wt.% Mo amount. From 25 wt.% Mo content, pure Mo was detected and proves the presence of unmelted Mo particles in the deposition. The last 100 wt.% Mo layers are pure molybdenum.

A modification of the lattice parameter between the substrate in Ti6Al4V and the 100 wt.% Mo deposition, as shown in Fig. 8, can also be noted. This lattice parameter was calculated with the Bragg relationship as defined in Eq. (2):

$$2dsin\theta = \lambda \tag{2}$$

where d is the interplanar spacing, θ is the Bragg angle, and λ is the x-ray wavelength (λ_{Co}=1.78 Å).

The value of the lattice parameter for the 100 wt.% Mo deposited (3.14 Å) is similar to the one found into the JCPDS data file 42–1120 (3.13 Å). The lattice parameter of the substrate in Ti6Al4V is 3.16 Å, which is close to the one found into the literature (3.19 Å) [17]. This value is lower than pure Ti (3.32 Å) [18] due to the presence of vanadium. An increase in the amount of Mo in the deposition leads to a decrease in the lattice parameter, which is consistent with the observations of Qiang [19]. The value of the lattice parameter of the gradient with both Ti6Al4V and Mo is lower than expected due to the presence of unmelted molybdenum particles.

The microstructural evolution of the Ti6Al4V-Mo alloy is shown in Fig. 9. The authors wish to focus on the difference in scales between the microstructures. As explained previously, Weiss et al. have shown that Ti6Al4 V deposited by CLAD® is principally composed of α' phase formed by the rapid cooling of columnar beta grains [20]. The microstructure of 100 wt.% Ti6Al4 V is principally α' martensitic with very small amount of β-phase (Fig. 9a). From 25 wt.% Mo the β-phase is predominant (Fig. 9b), which confirms the XRD results. Dendritic substructure is visible in β-grain for 50 wt.% and 75 wt.% Mo content (Fig. 9c-d). Many unmelted Mo particles were observed when Mo was introduced in the deposition. This can be explained by the insufficient energy density compared to the high molybdenum melting temperature. The amount of unmelted particles grows with the increase in Mo content. For 100 wt.% Mo (Fig. 9e), no unmelted particles were observed in the deposition due to the use of the highest energy density available with the laser. Unmelted Mo particle size distribution were estimated for the three gradients of composition depending on their diameter range (Fig. 9f-h). Results reveal that the majority of unmelted particles have between 20 and 30 μm diameter. For 75 wt.% Mo, there are twice many unmelted particles between 20 and 30 μm diameter as for the gradient with 50 wt.% Mo. Moreover, these results also allow to say that, in fact, these particles are partially melted. The initial sieved particle size distribution of Mo is 45-75 μm, while the residual particles size distribution of Mo in the deposition is 20-60 μm.

The morphological evolution of the grains along the direction of manufacturing is shown in Fig. 10. EBSD maps were performed at the interface of each gradient of chemical composition. The first transition (Fig. 10a) shows the interface between 100%Ti6Al4V

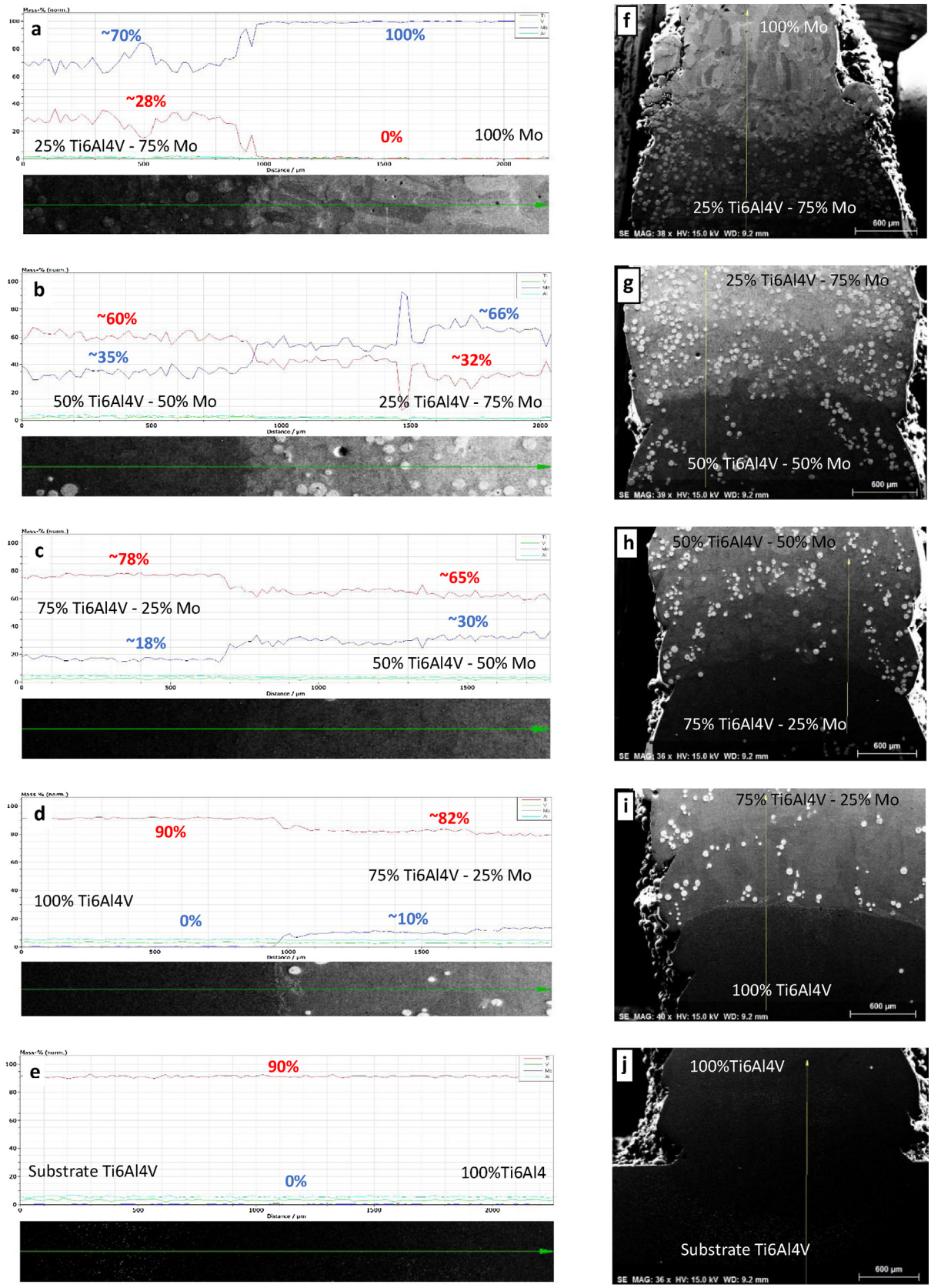

Fig. 4. EDS analysis of Ti6Al4V-Mo alloys from the top of the wall to the substrate with Ti6Al4V and Mo content wt.%. (a-e) variation in the chemical composition at the interface between two gradients (red curve: Ti, green curve: V, dark blue curve: Mo, light blue curve: Al) and (f-j) position of the measure. (For interpretation of the references to colour in this figure legend, the reader is referred to the web version of this article.)

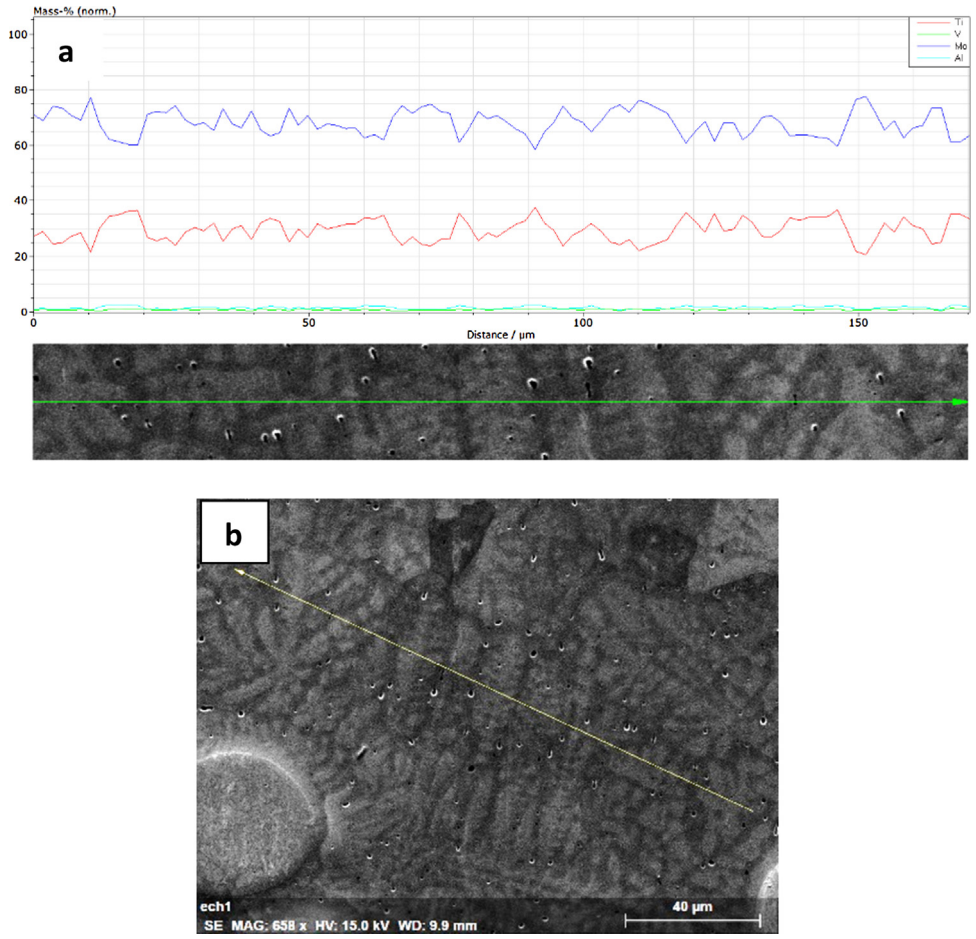

Fig. 5. EDS analysis of 25% Ti6Al4V-75% Mo wt.%. (a) variation in the chemical composition along the microstructure (red curve: Ti, green curve: V, dark blue curve: Mo, light blue curve: Al) and (b) position of the measure across the microstructure. (For interpretation of the references to colour in this figure legend, the reader is referred to the web version of this article.)

and 75%Ti6Al4V-25%Mo (in wt.%). The β-phase grain structure was reconstructed from the α-phase orientation map.

EBSD maps (Fig. 10a-d) show a perfect continuity of β-grain at the interface between each gradient of composition, revealing excellent metallurgical bonding. For 100 wt.% Ti6Al4V, coarse columnar β-grain grows parallel to the build direction, and a strong texture is visible as shown by the red colour in the IPF map, indicating a $\langle 100 \rangle_\beta$ fibre parallel to the build direction in accordance with the results of Antonysamy [21]. When Mo is introduced up to 25 wt.% of content, smaller columnar β-grains are observed, growing up parallel to the build direction, without specific crystallographic orientation compared to the previous 100 wt.% Ti6Al4V composition. Coarse equiaxed grains are also present in this gradient. Increasing the Mo content in the deposition leads to a morphological modification of the β-grains. Indeed, the columnar β-grains become equiaxed and the grain size distribution of equiaxed grains decreases from 10-200 µm for 25 wt.% Mo, to 5-60 µm for 75 wt.% Mo. Some authors have shown that equiaxed grains can nucleate and grow ahead of the moving solidification interface when there is a region of undercooled liquid. This can eventually lead to the transition from a columnar to an equiaxed dendritic morphology, referred to as CET (Columnar to Equiaxed Transition) [22–24].

Lines of very small equiaxed grains were observed at regular intervals along the wall manufacturing. The distance between two lines of this type corresponds to one track height. The remelting of the previous layer can lead to the hypothesis of the presence of these lines, and thus leads to the modification of grains morphology at the interface between two deposited tracks.

EBSD map also allows to check the crystallographic relation between the partially melted Mo particles in β-grains. The misorientation angle used to differentiate two adjacent grains was set to 10°. While two adjacent β-grains present a different crystallographic orientation, no significant orientation variation in an individual β-grain was observed (misorientation lower than 2°) in accordance with Almeida's works [11]. However, the misorientation profile across a partially melted Mo particle in a β-grain shows a slightly marked orientation (6° as show in Fig. 11). This result proves that, although some partially melted Mo particles are present with a slightly marked misorientation, they are included in the β-grain to which they belong.

4.4. Tomography

Tomography tests were performed to estimate the amount of partially melted Mo particles in the deposition. It also allows to know the spatial repartition of these partially melted particles, and thus the reparation of all elements, into the sample. Fig. 12 shows:

- the amount of partially melted Mo particles depending on the percentage of expected Mo
- the evolution of laser power parameter depending on the percentage of expected Mo

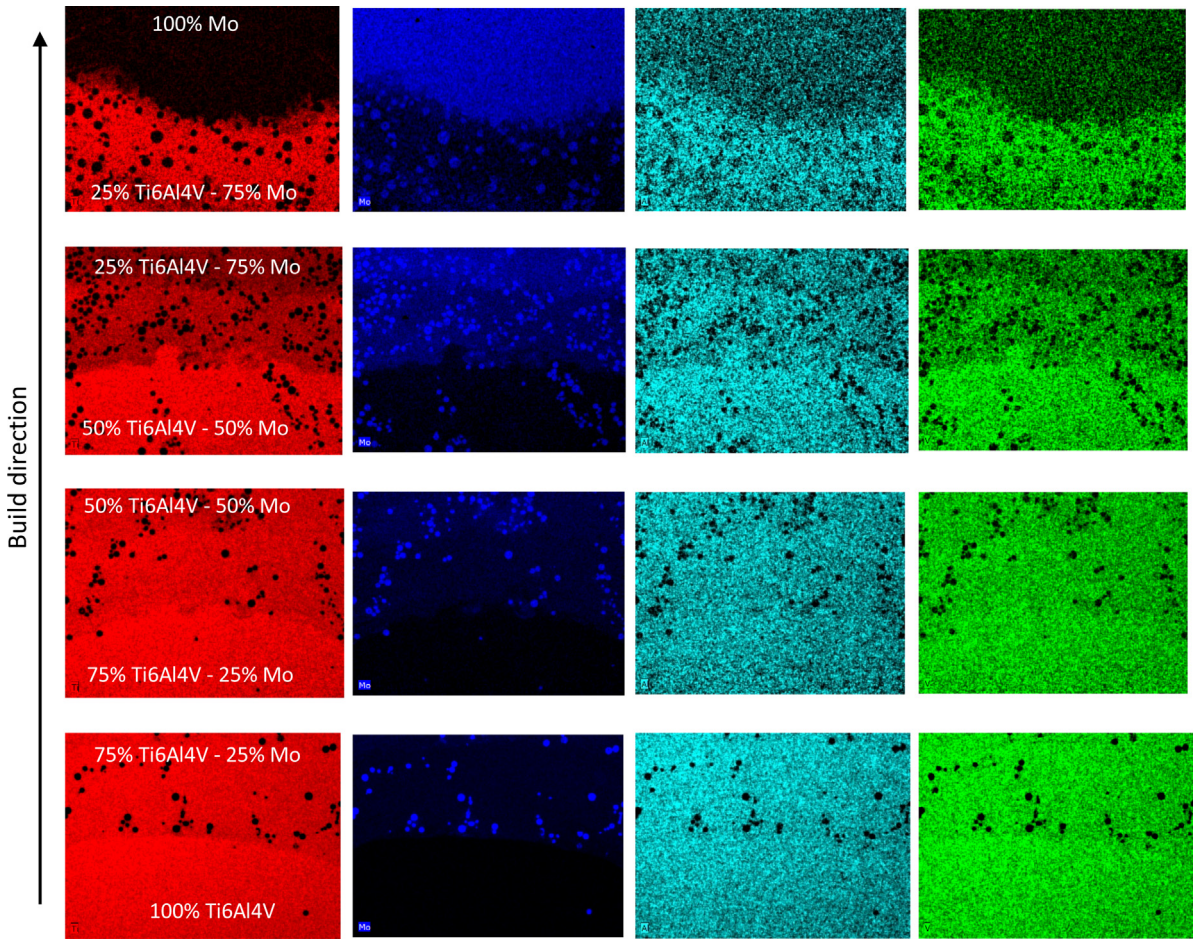

Fig. 6. EDS analysis of Ti6Al4V-Mo alloys from the top of the wall to the substrate with Ti6Al4V and Mo content (wt.%). Chemical distribution of Ti (red), Mo (dark blue), Al (light blue) and V (green) at the interface between two gradients depending on the chemical composition. (For interpretation of the references to colour in this figure legend, the reader is referred to the web version of this article.)

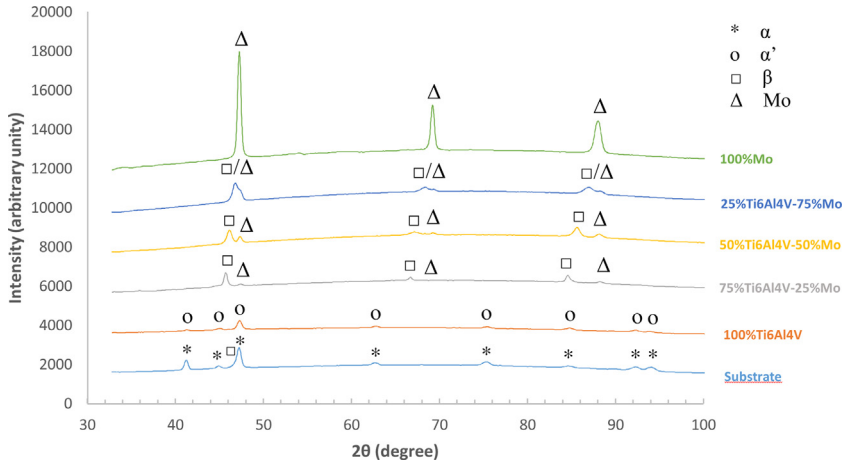

Fig. 7. X-ray diffraction patterns of Ti6Al4V-Mo alloys.

The blue curve (Fig. 12a) shows that the greater the amount of Mo programmed, the greater the number of partially melted Mo particles to be found in the deposited layer, except for 100 wt% Mo amount. Moreover, the orange curve (Fig. 12b) shows that the laser power was modified depending on the amount of Mo programmed.

During the construction, the laser power was adjusted depending on the chemical composition. When Mo is introduced from 25 wt.% to 75 wt%, laser power is increased up to 1800 W. However, this value still remains too low compared to the melting temperature of molybdenum to avoid partially melted particles ($T_{f(Mo)}$ = 2617 °C [25]). Up to 15% of partially melted Mo particles are measured in the gradient. For the last deposition with 100 wt.% Mo where the laser power is maximal (2000 W), no partially melted Mo particles were detected in the deposit. This involves that Mo particles could be fully melted by using a minimum power in the range of 1800-2000 W. Reducing the particle size distribution of Mo

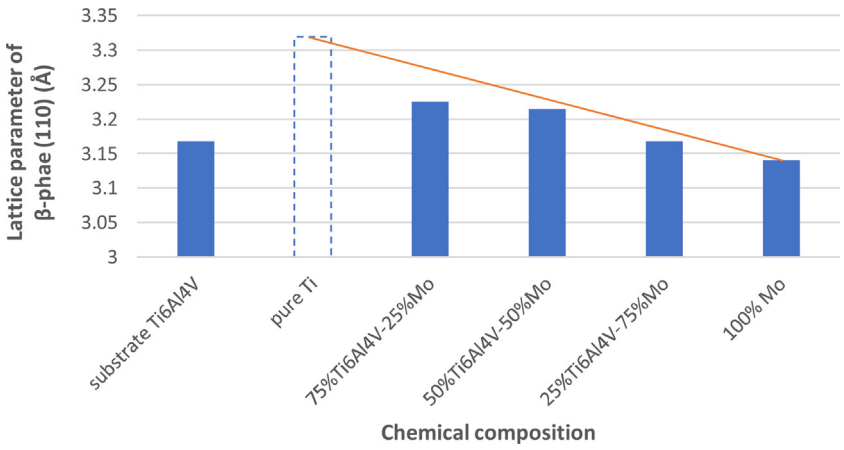

Fig. 8. Variation of the lattice parameter of the β-phase (110) depending on the chemical composition.

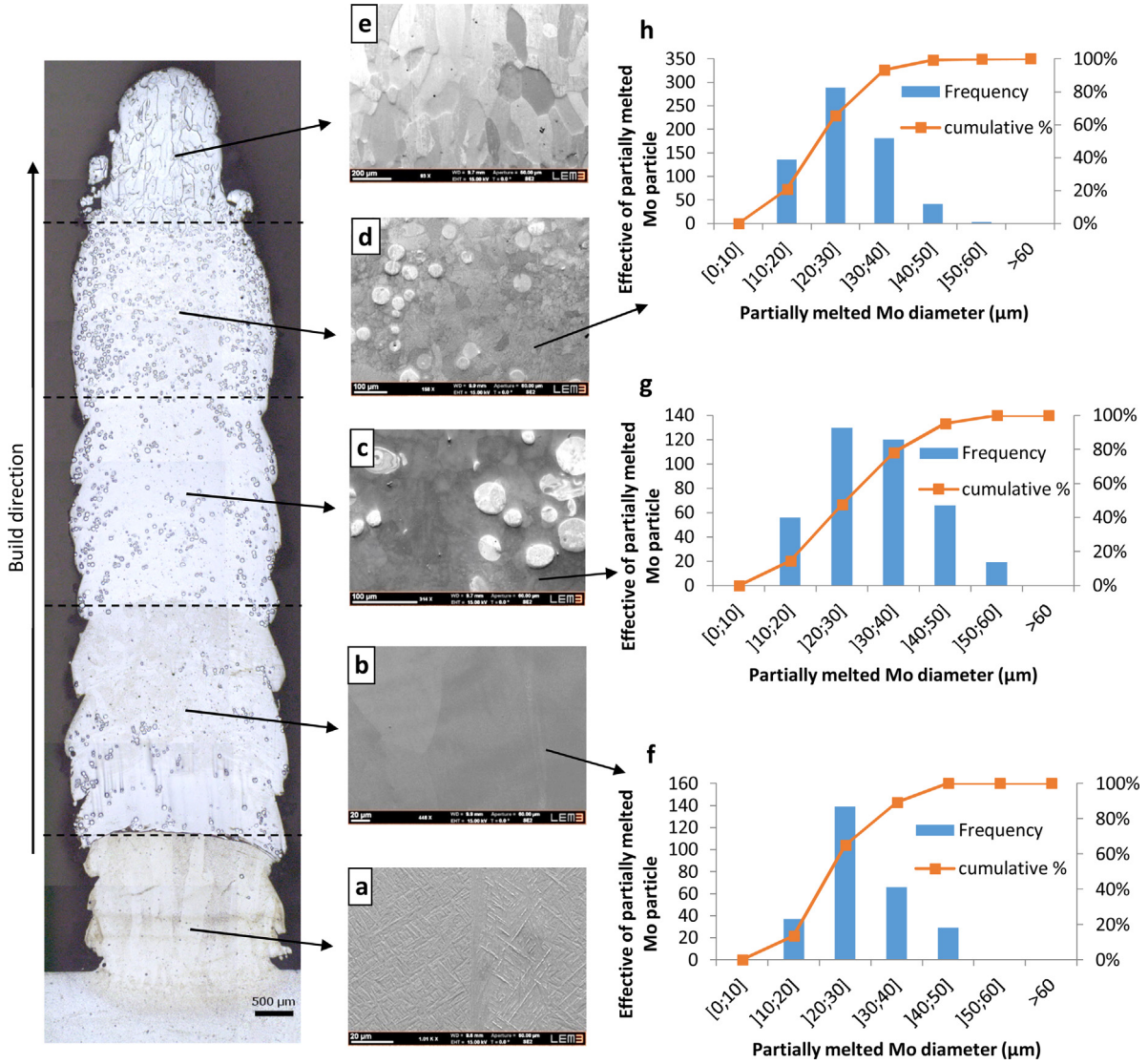

Fig. 9. Evolution of the microstructure of Ti6Al4V-Mo alloys with Mo content (wt.%) (a) 0% Mo, (b) 25% Mo, (c) 50% Mo, (d) 75% Mo, (e) 100% Mo. Partially melted Mo grain size distribution for (wt.%) (f) 25% Mo, (g) 50% Mo, (h) 75% Mo.

powder (<63 µm) could probably be an additional solution with the increase in laser power to reduce/avoid partially melted Mo particles in the deposit. Due to the absence of marked contrast between the matrix and the Mo partially melted on tomography results, it was not possible to measure the amount of partially melted particles for 75 wt.% Mo. Nevertheless, the amount of par-

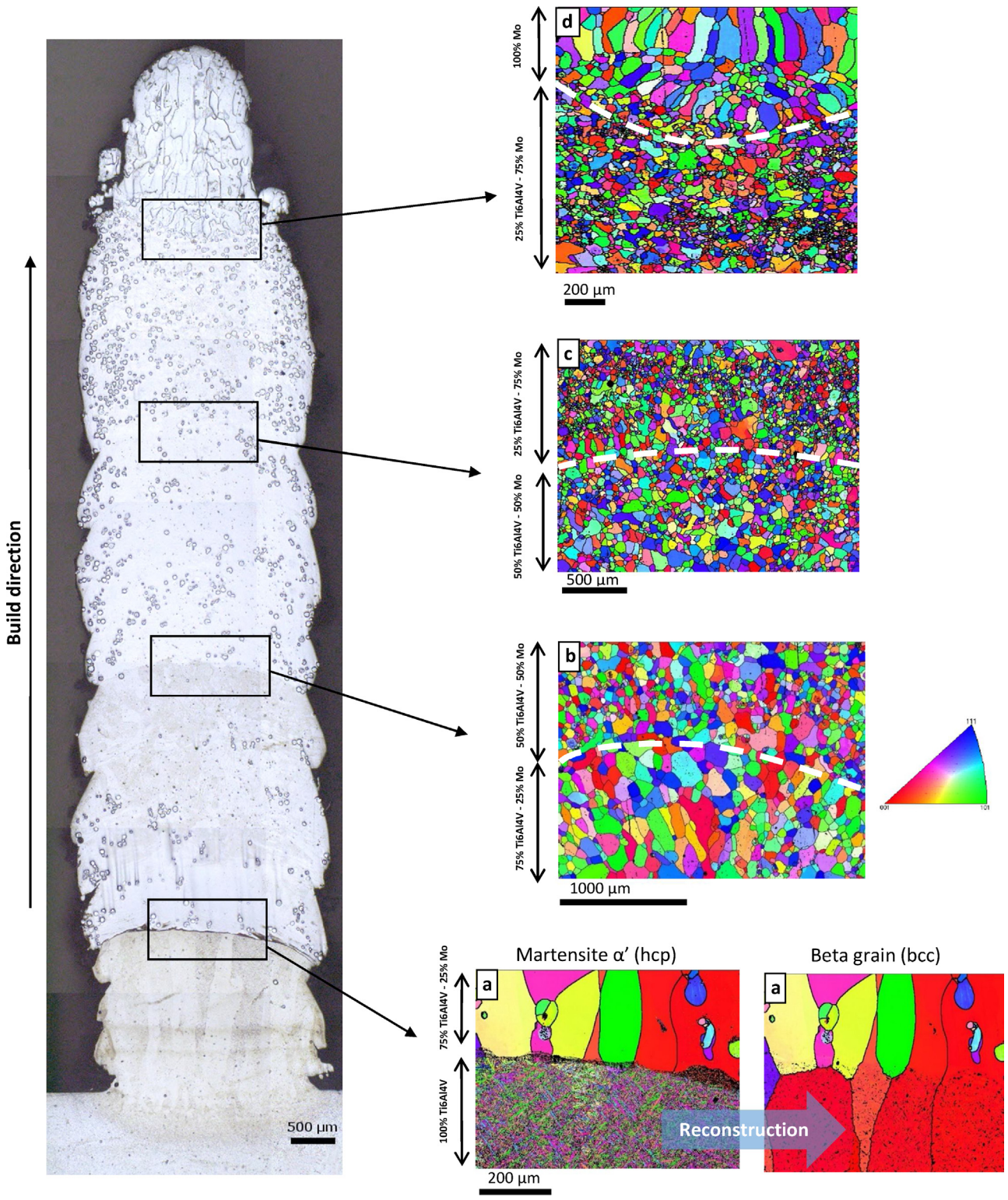

Fig. 10. IPF orientation coloured EBSD maps of Ti6Al4V-Mo alloys with Ti6Al4V and Mo content (wt%) at the interface between two gradients. (a) Measure before and after β-phase reconstruction at 100%Ti6Al4V/75%Ti6Al4V-25% Mo interface, (b-d) measured β-phase at three interfaces depending on the chemical composition. Broken lines correspond to interface between two gradients of composition.

tially melted Mo particles for this composition could be expected to be found from ~20% considering the linearity of the three previous points. Tomography results also show that partially melted Mo has homogenous distribution in the observed volume (see video 1 given with the article).

4.5. Microhardness

Microhardness measurements were performed using a Vickers microhardness indentor. Fig. 13 shows the microhardness variation as a function of the sample length from the baseplate to the top of the wall. Three measurement lines made of different width and sep-

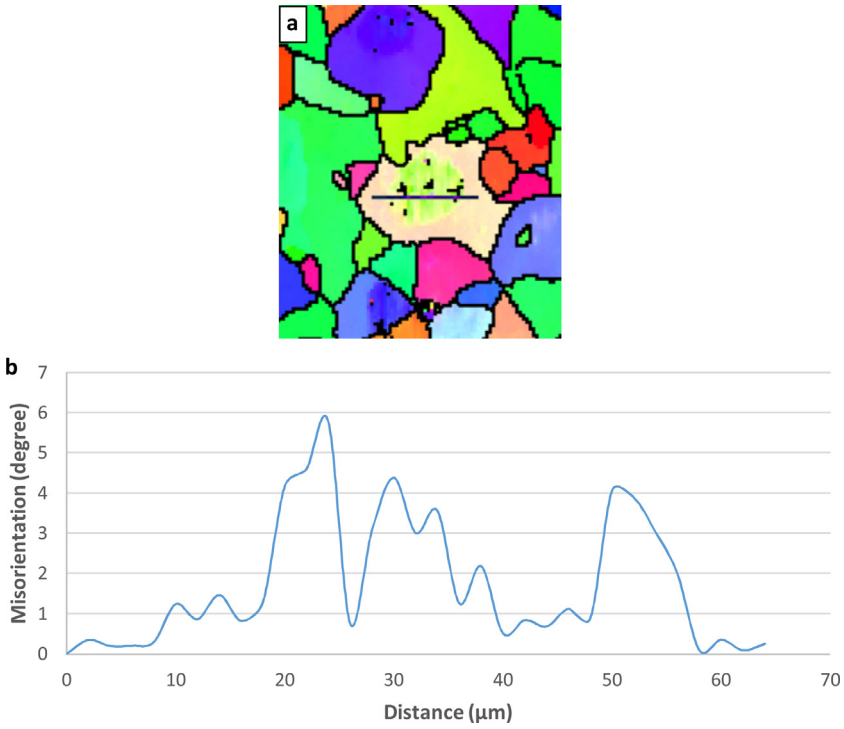

Fig. 11. (a) EBSD orientation map in 50%Ti6Al4V-50% Mo wt.% alloy; (b) misorientation profile across a partially melted Mo particle included in a beta grain.

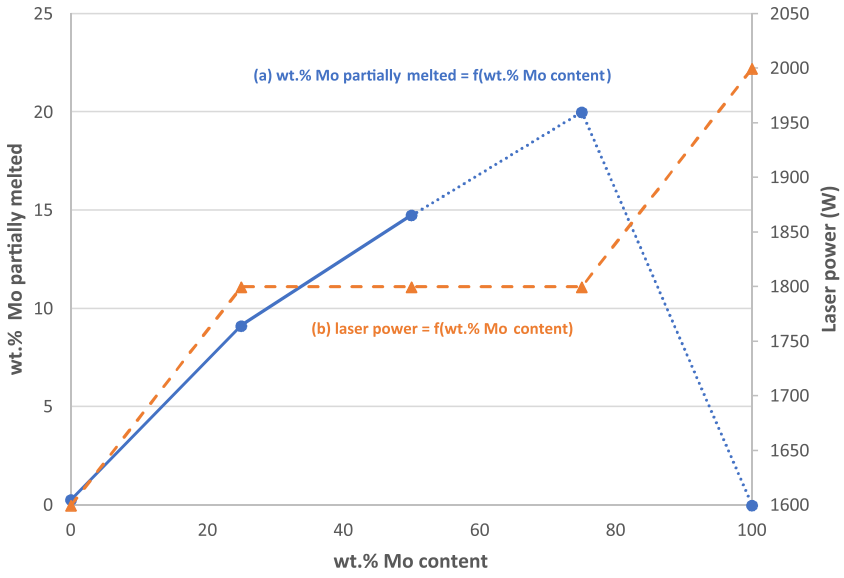

Fig. 12. (a) evolution of the partially melted Mo particles along the construction, (b) evolution of the laser power depending on the Mo amount programming.

arated by 0.75 mm were performed. Each indentation is separated by 0.33 mm in the manufacturing build direction. Fig. 13a revealed a very heterogeneous result. Microhardness increases from 250 to 450 HV when molybdenum is introduced, before dropping to 190 HV for pure molybdenum. The hardness in the substrate was found around 295 HV, slightly lower than conventional Ti6Al4V (350 HV) [26]. The hardness in the first Ti6Al4V layer deposited increased up to around 390 HV, probably due to the rapid cooling of this deposition in contact with cold substrate. During the Ti6Al4V deposition along the wall, hardness stabilized around 345 HV, which is consistent with the literature. When up to 25 wt.% Mo was introduced, hardness decreased to around 265 HV before gradually increasing again until 50 wt.% Mo amount was reached. Recent works on Ti-Mo alloy show a peak of hardness value up to 450 HV for 10 wt.% Mo before decreasing to around 300 HV for 20 wt.% Mo (the maximum Mo amount introduced in these works) [12]. Collins et al. explained this hardness peak value by the modification of the volume fraction of the β-phase which is higher than that of the α-phase, but also by a microstructure consisting of a fine dispersion of α precipitates within the β matrix.

As no data are reported in literature for alloys with more than 20 wt.% Mo, it is difficult to explain the hardness evolution from 25 wt.% to 100 wt.% Mo, as well as the scattering variation for gradient with 75 wt.% Mo. For 75 wt.% Mo amount, the hardness scattered from 385 to 450 HV. The lowest value (below to 350 HV) is explained by the indentation that was performed on or at the vicin-

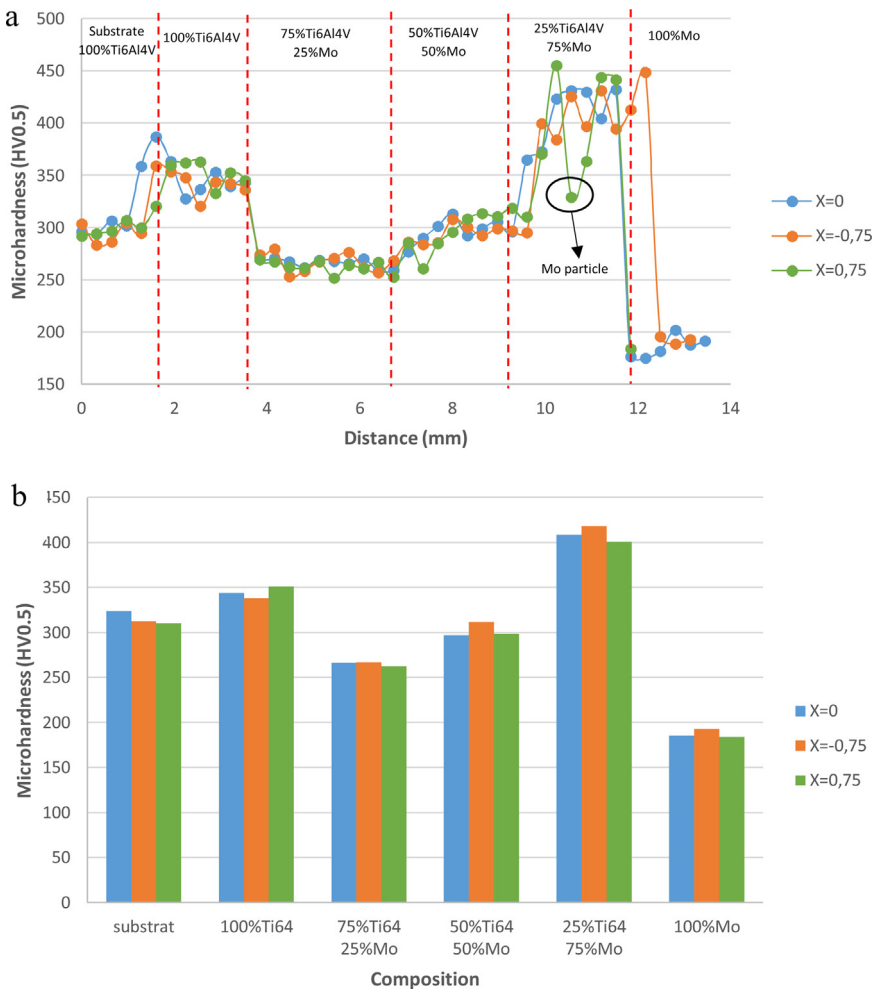

Fig. 13. (a) Variation in the microhardness of Ti6Al4V-Mo alloys from the substrate to the top of the wall, (b) average measurement for each gradient of composition.

ity of partially melted Mo particles, which is softer than the Ti6Al4V area. The possible formation of Mo_3Al intermetallic in the deposition may justify this high hardness scattering [13,27]. Further works are ongoing to explain the relationship between hardness and microstructure. The last deposited layers with 100 wt.% Mo shows a hardness value around 190 HV, which is slightly lower than conventional annealed Mo (230 HV).

5. Conclusion

This work allowed to highlight the processability of FGMs system with the DED-CLAD® process, with a demonstration for the Ti6Al4V-Mo system. Several conclusions can be outlined:

- In this study, functionally graded Ti6Al4V-Mo alloys were successfully manufactured with DED-CLAD® process. A specimen was manufactured with several incremental increases of 25 wt% of Mo in Ti6Al4V, starting from 100% Ti6Al4V at the base of the construction to reach 100% Mo at the top of the construction.
- There is satisfactory metallurgical bonding between the deposit and the substrate, but also between each deposited layer.
- Tomography and chemical analysis have confirmed the uniformity of the powder mixture before being melted under the laser beam. Thus, the homogeneity of the powder mixture was validated.
- Microstructural results have shown an evolution in the microstructure along the deposition build direction, as shown by the transformation of coarse columnar beta grains to equiaxed grains. The size distribution of equiaxed grains decreases with the increase in molybdenum content.
- Microhardness varied along the deposition due to the increase in molybdenum amount. Minimum value (265 HV) is reached for 25 wt.% Mo amount, while maximum value (450 HV) is attained for 75 wt.% Mo amount. The microhardness of pure Ti6Al4V is around 345 HV, and around 190 HV for pure molybdenum. The modification of the microstructure is responsible for the variation in the microhardness throughout manufacturing.
- Future works are ongoing to reduce/avoid partially melted Mo particles in the deposition. Another chemical composition will be tested with 15% or 10% increment between each gradient.

As this work allowed to validate the manufacture of FGMs with the DED-CLAD® process, future work is ongoing on other metallurgical systems. Tests were performed to manufacture walls with Ti6Al4V-Inconel 718 alloys. The study of this system is very complex due to the formation of intermetallic phases for a given Inconel 718 amount. However, this alloy opens up opportunities for new applications for aerospace industry.

Acknowledgment

The authors acknowledge MBDA company as industrial partner, especially Sébastien DAVID from MBDA France and Mike KEMP from MBDA UK for the support of this work.

Appendix A. Supplementary data

Supplementary data associated with this article can be found, in the online version, at http://dx.doi.org/10.1016/j.addma.2017.07.008.

References

[1] C. Margueray, L. Vollard, Fabrication Additive Metallique Technologie et opportunites, INSA, Rouen, 2015, INSA report, in French.
[2] D.D. Gill, J.E. Smugeresky, C.J. Atwood, Laser Engineered Net Shaping™(LENS®) for the Repair and Modification of NWC Metal Components, Sandia National Laboratories, 2006, SANDIA report.
[3] M. Naebe, K. Shirvanimoghaddam, Functionally graded materials: a review of fabrication and properties, Appl. Mater. Today 5 (2016) 223–245.
[4] D.C. Hofmann, et al., Developing gradient metal alloys through radial deposition additive manufacturing, Sci. Rep. 4 (2014) 1–8.
[5] B.E. Carroll, et al., Functionally graded material of 304L stainless steel and inconel 625 fabricated by directed energy deposition: characterization and thermodynamic modeling, Acta Mater. 108 (2016) 46–54.
[6] M. Niinomi, Mechanical biocompatibilities of titanium alloys for biomedical applications, J. Mech. Behav. Biomed. Mater. 1 (1) (2008) 30–42.
[7] Y. Okazaki, et al., Corrosion resistance, mechanical properties, corrosion fatigue strength and cytocompatibility of new Ti alloys without Al and V, Biomaterials 19 (13) (1998) 1197–1215.
[8] K. Shah, et al., Experimental study of direct laser deposition of Ti-6Al-4V and inconel 718 by using pulsed parameters, Sci. World J. 2014 (2014) 1–6.
[9] M.S. Domack, J.M. Baughman, Development of nickel-titanium graded composition components, Rapid Prototyping J. 11 (1) (2005) 41–51.
[10] J. Fessler, et al., Functional gradient metallic prototypes through shape deposition manufacturing, Proceedings of the Solid Freeform Fabrication Symposium (1997) 521–528.
[11] A. Almeida, et al., Laser-assisted synthesis of Ti-Mo alloys for biomedical applications, Mater. Sci. Eng. C 32 (5) (2012) 1190–1195.
[12] P.C. Collins, et al., Laser deposition of compositionally graded titanium-vanadium and titanium-molybdenum alloys, Mater. Sci. Eng. A 352 (1–2) (2003) 118–128.
[13] M. Humbert, N. Gey, The calculation of a parent grain orientation from inherited variants for approximate (bcc-hcp) orientation relations, J. Appl. Crystallogr. 35 (4) (2002) 401–405.
[14] V. Fallah, S.F. Corbin, A. Khajepour, Solidification behaviour and phase formation during pre-placed laser cladding of Ti45Nb on mild steel, Surf. Coat. Technol. 204 (15) (2010) 2400–2409.
[15] W.F. Ho, C.P. Ju, J.H. Chern Lin, Structure and properties of cast binary TiMo alloys, Biomaterial (1999) 2115–2122.
[16] Y. Robert, Simulation numérique du soudage du TA6V par laser YAG impulsionnel: caractérisation expérimentale et modélisation des aspects thermomécaniques associés à ce procédé, École Nationale Supérieure des Mines de Paris, 2007, in french.
[17] Y. Combres, Traitement thermique des alliages de titane, 2013.
[18] Y.A.O. Qiang, et al., Influence of Nb and Mo contents on phase stability and elastic property of β-type Ti-X alloys, Trans. Nonferrous Met. Soc. China 17 (6) (2007) 1417–1421.
[19] L. Weiss, et al., Microtexture of Ti6Al4 V obtained by direct energy deposition (DED) process, Proceeding of the 13th World Conference on Titanium (2016) p. 1305–1310.
[20] A.A. Antonysamy, J. Meyer, P.B. Prangnell, Effect of build geometry on the β-grain structure and texture in additive manufacture of Ti6Al4 V by selective electron beam melting, Mater. Charact. 84 (2013) 153–168.
[21] M. Gäumann, R. Trivedi, W. Kurz, Nucleation ahead of the advancing interface in directional solidification, Mater. Sci. Eng. A 226 (1997) 763–769.
[22] J.D. Hunt, Steady state columnar and equiaxed growth of dendrites and eutectic, Mater. Sci. Eng. 65 (1) (1984) 75–83.
[23] J. Lipton, W. Heinemann, W. Kurz, Columnar to equiaxed transition (CET) in castings – Part 1: determination of the CET from cooling curves, Eisenhüttenwes 55 (1984) 195–200.
[24] F. Maratray, Molybdene et ses alliages, Technique de l'Ingérieur, 1992, n° M2374, in french.
[25] ASM International, Properties and selection: nonferrous alloys and special-purpose materials ASM Handbook, vol. 2, 1990.
[26] ASM International, Alloy phase diagrams ASM Handbook, vol. 3, 2001.
[27] E. Svanidze, et al., High hardness in the biocompatible intermetallic compound –Ti3Au, Sci. Adv. 2 (7) (2016).